Shapes of grain inclusions in crystals

Y. He, C. Jayaprakash, and Craig Rottman
Department of Physics and The Materials Research Laboratory, The Ohio State University, Columbus, Ohio 43210
(Received 2 August 1984; revised manuscript received 1 April 1985)

The "equilibrium" shape of a grain (with fixed volume) embedded in a simple-cubic crystal of the same material and rotated by a small angle with respect to the [001] axis is studied. The dislocation model of grain boundaries of Read and Schockley is used to compute the grain-boundary energy as a function of orientation. The grain shape is then found from this energy via the Wulff construction. Various aspects of the shape are analyzed for different values of both Poisson's ratio ν and a constant characterizing the core energy. One novel feature in this zero-temperature shape is curved portions which meet facets at edges where there is a discontinuity in slope. For small ν the shape is essentially a smoothly curved ellipsoid of revolution with four equivalent elliptical facets on the (100), (010), ($\bar{1}$00), and (0$\bar{1}$0) planes. For large values of ν two smooth parts can meet at the equatorial plane with a slope discontinuity. In phase-transition language we find, besides first-order transitions, triple points and, in a narrow regime in ν, critical points. Effects of nonzero temperature and the dependence of the core energy on the character of the dislocation are explored qualitatively.

I. INTRODUCTION

When two bulk phases coexist a macroscopic inclusion of one phase can remain in stable equilibrium with the other "background" phase. The shape of such an inclusion is determined by minimizing the total free-energy cost of creating the interfacial boundaries for a fixed volume of the inclusion. If both phases are isotropic, the interfacial free energy is independent of the orientation and the inclusion is spherical. If the included phase is anisotropic (crystal) and the second phase is isotropic (vapor), the broken rotational invariance of the crystal leads to orientation dependence of the interfacial free energy. The corresponding shape is less trivial, including facets and/or curved surfaces. Such equilibrium crystal shapes (ECS) have been studied extensively both theoretically[1–3] and experimentally.[4] In this paper we are concerned with the problem of determining the shape when *both* the inclusion and the background are crystalline. In particular, we consider the situation in which a grain, composed of the same material as the background, is rotated by a *small* angle with respect to one of the background symmetry axes. We perform what is, to the best of our knowledge, the first quantitative calculation of the shape of a grain at zero temperature. We also explore the effects of finite temperature qualitatively.

At the outset we should note that the formulation of our problem contains conceptual difficulties in addition to those of the venerable ECS problem mentioned in Ref. 1. In the ECS problem the inclusion may be stabilized by fixing the number of particles in the container which encloses both phases. Since the two phases have, in general, different densities, it is possible to create a macroscopic crystallite of the desired size with a time-independent shape. On the other hand, there seems to be no physical constraint in our problem which prevents the inclusion from rotating back into alignment with the background and, thus, losing its identity. Even though the creation of an *equilibrium* (time-independent) grain appears unlikely, metastable grains may be formed in the crystal growth process. For our considerations to be applicable the grain boundaries must reach equilibrium under the constraint of fixed volume. On the time scale of observation, macroscopic (bulk) diffusion processes can be sufficiently slow that the fixed volume condition is satisfied. Ideal grain boundaries whose motion usually involves *local* rearrangement of atoms can reach equilibrium and our calculated "equilibrium" shapes may indeed correspond to experimentally observable shapes. Such ideas on the application of our results to experiments are merely intuitive; a proper understanding of such metastable inclusions, though important, is lacking at this time.

To compute the shape at $T=0$ K we first need the interfacial energy as a function of orientation. We now describe the model within which this computation is performed. Since a grain boundary is the interface where two single crystals of different orientation join, its energy E is a function of five variables:[5–7] the relative orientation of the two crystal (this involves three parameters, such as $\hat{\mathbf{u}}$, the axis of rotation, and δ, the angle of rotation) and the orientation of the boundary surface itself, specified by its normal $\hat{\mathbf{n}}$ (two parameters). Four additional variables which describe the translation between the two crystals and the exact placement of the interface between the two grains may be defined but are neglected here, since in practice they are usually allowed to relax to equilibrium. When the orientation difference δ between the crystals is small it is possible to join the two crystals with a suitable array of dislocations lying in the prescribed plane of the grain boundary. This dislocation density increases with increasing misorientation until, for large δ, the dislocation cores overlap and the dislocation-network picture breaks down. However, for low-angle grain boundaries, i.e., small misorientation δ, there is ex-

tensive experimental evidence to support the validity of dislocation models.[6,8] Following Bragg and Burgers, Read and Shockley[5] (RS) showed that the dislocation model can be used quantitatively to calculate the grain-boundary energy $E(\hat{\mathbf{n}})$ for low-angle asymmetric tilt boundaries $[\hat{\mathbf{u}}=\hat{\mathbf{z}},\hat{\mathbf{n}}=(\cos\phi,\sin\phi,0)]$ in a simple-cubic crystal. In this case the boundary consists of two parallel nonoverlapping sets of edge dislocations. To obtain $E(\hat{\mathbf{n}})$ for arbitrary $\hat{\mathbf{n}}$ for fixed small δ and $\hat{\mathbf{u}}=\hat{\mathbf{z}}$, we need to know the dislocation content of such a boundary. This can be done by using Frank's formula[6,7] as explained in Sec. III A. In our problem we find that two sets of mixed dislocations forming a lozenge-shaped mesh are required for general $\hat{\mathbf{n}}$.

Knowing the geometry of the dislocation mesh for a given boundary orientation $\hat{\mathbf{n}}$, the energy per unit area is calculated within linear elasticity theory following RS.[5] This is done by determining the energy required to create the dislocations and the work done in bringing them together due to the interactions between them. An outline of the calculations is sketched in Sec. III B with the details relegated to the Appendix. The calculation leads to the energy of the grain boundary of the following form:

$$E(\hat{\mathbf{n}})=(\tau_0 b^2/2)E_0\delta(A-\ln\delta)\,, \tag{1.1}$$

where $\tau_0=G[2\pi(1-\nu)]^{-1}$ (G is the shear modulus and ν is Poisson's ratio), b is the magnitude of the Burgers vector, and E_0 and A are dimensionless functions of $\hat{\mathbf{n}}$. A typical (large-δ) value of E is 10^3 ergs/cm^2, while A lies between 0.1 and 0.5.[8]

Given $E(\hat{\mathbf{n}})$, the grain shape can be calculated in time-honored fashion using the Wulff construction[9] (Sec. II). We now provide a brief summary of the results of such a calculation. (For a detailed discussion, see Sec. IV.)

For small ν [Fig. 1(a)] the shape is approximately an ellipsoid of revolution truncated by four elliptical facets on the (100), ($\bar{1}$00), (010), and (0$\bar{1}$0) planes. The four facets arise from four equivalent cusps in $E(\hat{\mathbf{n}})$ at $\hat{\mathbf{n}}=(\pm1,0,0),(0,\pm1,0)$, as explained in Secs. II and IV. The rest of the grain is smoothly rounded, a feature *not* found in previous ECS calculations at $T=0$. This difference in our problem arises because we use a continuum model in which long-range forces are present. In particular, the spacing between the dislocations D is treated as a continuous variable and the underlying lattice structure is ignored. For δ and $\hat{\mathbf{n}}$ corresponding to D being an integer or rational multiple of a lattice constant, cusps in E will occur as noted in RS. However, for small δ (large D) these cusps are weak.[5] Furthermore, either thermal fluctuations or experimental-resolution effects will wash out these cusps which we have ignored.

Another interesting aspect of the shape is that the facet-to-curved-surface transition is first order in the sense that there is a slope discontinuity at the edge where they meet. In ECS models a *continuous* transition at such an edge has been noted.[1,3,10] This difference is due to the fact that, in contrast to step energies in ECS models which are finite, the dislocation energy per unit length in the grain problem is logarithmically divergent with the size of the system.[6,7]

Now consider larger values of the Poisson's ratio ν.

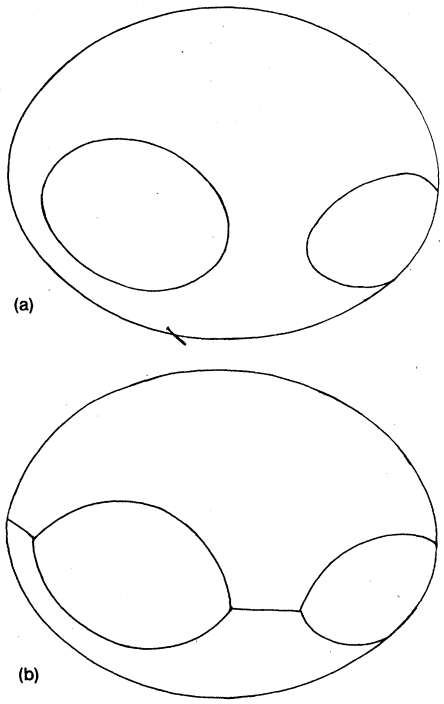

FIG. 1. Sketches of a grain inclusion in which Poisson's ratio ν is (a) small and (b) large. In both cases four symmetry related facets, with normals (100), (010), ($\bar{1}$00), and (0$\bar{1}$0), meet the smoothly curved region with discontinuous tangents. A good approximation to (a) is an ellipsoid of revolution truncated by four elliptical facets. In case (b) the smoothly curved region above the equatorial plane meets its counterpart below the equatorial plane with slope discontinuity.

For large ν the schematic shape is displayed in Fig. 1(b). An interesting new feature is that when the smoothly curved parts meet at the equatorial plane, the slope is discontinuous. For intermediate values of ν we find both slope discontinuity and no slope discontinuity at the equator, interpolating between Figs. 1(a) and 1(b). In phase-transition language the intermediate-ν regime is especially rich (see Sec. IV C).

Our calculation has several limitations: it holds only for small rotations about symmetry axes; it assumes the often unrealistic simple-cubic-lattice structure; it neglects the $\hat{\mathbf{n}}$ dependence of the core energy as well as thermal and impurity effects; and it assumes that the grain is very large and composed of the same material as the background. In Sec. V we discuss both the seriousness of these limitations and possible extensions of our work which connect more directly with experiments. Qualitative predictions are made for the incorporation of both the $\hat{\mathbf{n}}$ dependence of the core energy and thermal effects.

The outline of this paper is as follows. We recapitulate the Wulff construction in Sec. II. Section III A contains a discussion of Frank's formula and its application to our problem. In Sec. III B we outline the calculation of the grain-boundary energy. A detailed discussion of the grain shape can be found in Sec. IV. We comment in Sec. V on

the effects of features which may be important in experiments but are ignored in our calculation. The Appendix provides details of the calculation discussed in Sec. III.

II. THE WULFF CONSTRUCTION

The equilibrium shape of an inclusion is obtained by minimizing the surface integral of the interfacial free energy subject to the constraint of constant volume. Mathematically one minimizes

$$\int E(\hat{\mathbf{n}})ds - 2\lambda \int dv \ ,$$

where 2λ is the Lagrange multiplier and $E(\hat{\mathbf{n}})$ is the interfacial free energy for orientation $\hat{\mathbf{n}}$. This leads to the Wulff construction[11] for $R(\hat{\mathbf{r}})$, the radius of the equilibrium shape of the inclusion along the direction $\hat{\mathbf{r}}$; analytically, this is given by

$$\lambda R(\hat{\mathbf{r}}) = \min_{\hat{\mathbf{n}}} E(\hat{\mathbf{n}})/(\hat{\mathbf{n}}\cdot\hat{\mathbf{r}}) \ . \tag{2.1}$$

Geometrically, it yields the elegant Wulff construction described in textbooks:[12] Make a polar plot of $E(\hat{\mathbf{n}})$ as a function of $\hat{\mathbf{n}}$ (the Wulff plot). Draw a radius in the direction $\hat{\mathbf{n}}$ from the origin to the Wulff plot. Construct a plane orthogonal to $\hat{\mathbf{n}}$ and passing through the point of intersection of the radius with the Wulff plot. The interior envelope of all such planes (for all $\hat{\mathbf{n}}$) yields the "equilibrium inclusion shape." Cusps in the Wulff plot lead naturally to extended planar regions which we term facets in the case of the grain inclusion also. A detailed discussion of various aspects of the Wulff construction can be found in Refs. 1 and 13.

The curved parts of $R(\hat{\mathbf{r}})$ follow from $E(\hat{\mathbf{n}})$ by the use of the following equations:

$$X = E\sin\theta\cos\phi + \cos\theta\cos\phi\frac{\partial E}{\partial\theta} - \frac{\sin\phi}{\sin\theta}\frac{\partial E}{\partial\phi} \ , \tag{2.2a}$$

$$Y = E\sin\theta\sin\phi + \cos\theta\sin\phi\frac{\partial E}{\partial\theta} + \frac{\cos\phi}{\sin\theta}\frac{\partial E}{\partial\phi} \ , \tag{2.2b}$$

$$Z = E\cos\theta - \sin\theta\frac{\partial E}{\partial\theta} \ , \tag{2.2c}$$

where

$$\hat{\mathbf{n}} = (\sin\theta\cos\phi, \sin\theta\sin\phi, \cos\theta) \tag{2.3}$$

and X, Y, Z are the Cartesian coordinates of the inclusion.

These equations are obtained by performing the minimization indicated in Eq. (2.1) explicitly. They relate the curved part of $E(\hat{\mathbf{n}})$, where the derivatives of Eq. (2.2) exist, to the curved parts of $R(\hat{\mathbf{r}})$. Defining

$$\hat{\mathbf{r}} = (\sin\Theta\cos\Phi, \sin\Theta\sin\Phi, \cos\Theta) \ , \tag{2.4}$$

$R(\hat{\mathbf{r}})$ is given by

$$\lambda R = (X^2 + Y^2 + Z^2)^{1/2} \ , \tag{2.5a}$$

$$\cos\Theta = Z/R \ , \tag{2.5b}$$

$$\tan\Phi = Y/X \ . \tag{2.5c}$$

The special case of these for two dimensions can be found in the classic paper of Burton, Cabrera, and Frank.[14]

Note that, for a given direction $\hat{\mathbf{r}}$, there can be multiple solutions to (2.2) and (2.5), i.e., different points on the Wulff plot contribute to the same $\hat{\mathbf{r}}$ as extrema, leading to spurious curved parts.[15] One must use the minimum (smallest R) among these solutions. Thus, knowing $E(\hat{\mathbf{n}})$ we can determine the shape of the inclusion $R(\hat{\mathbf{r}})$.

III. CALCULATIONS

A. Application of Frank's formula

In this subsection we derive the dislocation geometry of an infinite grain boundary with an arbitrary orientation $\hat{\mathbf{n}}$ for rotation around the $\hat{\mathbf{z}}$ axis. Frank's formula states[6,7]

$$\mathbf{d} = 2(\mathbf{r}\times\hat{\mathbf{u}})\sin(\delta/2) \ , \tag{3.1}$$

where $\mathbf{r}$ is an arbitrary vector lying in the plane of the boundary, $\mathbf{d}$ is the sum of the Burgers vectors of the dislocations intersected by $\mathbf{r}$, and δ is the angle of rotation around the axis denoted by $\hat{\mathbf{u}}$.

It is instructive to provide a derivation of (3.1) for small δ.[6,7] Consider two grains A and B rotated with respect to each other by δ around $\hat{\mathbf{u}}$. Let the plane of the boundary be specified by its normal $\hat{\mathbf{n}}$. Consider an arbitrary vector $\mathbf{r}$ in the plane of the boundary. Let $\mathbf{r}'$ have the same indices with respect to B that $\mathbf{r}$ has in A, with a common origin. For small δ, a rotation $\delta\hat{\mathbf{u}}$ brings A and B into coincidence making $\mathbf{r}$ and $\mathbf{r}'$ identical. Hence, we have

$$\mathbf{r}' = \mathbf{r} + \delta(\hat{\mathbf{u}}\times\mathbf{r}) \ . \tag{3.2}$$

Now perform the Burgers circuit connecting $\mathbf{r}$ and $\mathbf{r}'$ and their origin. The closure failure of the end points of $\mathbf{r}-\mathbf{r}'$ is obviously the sum $\mathbf{d}$ of the Burgers vectors of the dislocation lines enclosed by the circuit, i.e., cut by $\mathbf{r}$. Hence we have Eq. (3.1), with $2\sin(\delta/2)\to\delta$.

Since $\mathbf{d}$ is proportional to $|\mathbf{r}|$ for arbitrary orientations of $\mathbf{r}$ in the boundary plane, the grain boundary is made up of sets of uniformly spaced parallel dislocations which are macroscopically straight. Note that the dislocation density is proportional to δ for small δ. The number of geometrically allowed models is equal to the number of ways of resolving a given $\mathbf{d}$ into the appropriate Burgers vectors $\mathbf{b}_i$. In principle, one must calculate the energy for all possible realizations and choose the lowest energy configuration.[6,7]

By making different choices for $\mathbf{r}$ in (3.1) the geometry of the dislocations can be determined. For the case of three sets of dislocations $\mathbf{d}$ is given by

$$\mathbf{d} = c_1\mathbf{b}_1 + c_2\mathbf{b}_2 + c_3\mathbf{b}_3 \ , \tag{3.3}$$

where the $\mathbf{b}_i$ are the Burgers vectors (noncoplanar) and $c_i(\mathbf{r})$ are the number of dislocations lines with Burgers vectors $\mathbf{b}_i$ intersected by $\mathbf{r}$. Let $\hat{\mathbf{r}}_i$ be the sense vector (direction) of the ith set of dislocation lines. If we chose $\mathbf{r} = \mathbf{r}_1 = |\mathbf{r}|\hat{\mathbf{r}}_1$, then $c_1(\mathbf{r}_1) = 0$ since $\mathbf{r}$ is parallel to the corresponding dislocation lines. Thus

$$\mathbf{r}_1\times\hat{\mathbf{u}}\delta = c_2\mathbf{b}_2 + c_3\mathbf{b}_3 \ . \tag{3.4}$$

Also $\mathbf{r}_1\cdot\hat{\mathbf{n}} = 0$ since $\mathbf{r}_1$ lies along the boundary. Thus we obtain

$$\mathbf{r}_1 \propto \hat{\mathbf{n}}\times[\hat{\mathbf{u}}\times(\mathbf{b}_2\times\mathbf{b}_3)] \ . \tag{3.5}$$

The dislocation density $\rho_1 = c_1(\mathbf{r})/|\mathbf{r}|$, where $\mathbf{r}$ lies in the boundary plane and is normal to $\mathbf{r}_1$. Choosing $\hat{\mathbf{r}}||\hat{\mathbf{r}}_1\times\hat{\mathbf{n}}$ it is easy to show that

$$\rho_1 = \delta\,|\,\hat{\mathbf{n}}\times(\mathbf{b}_1^*\times\hat{\mathbf{u}})\,| \ , \tag{3.6}$$

where $\mathbf{b}_1^* = (\mathbf{b}_2\times\mathbf{b}_3)/[\mathbf{b}_1\cdot(\mathbf{b}_2\times\mathbf{b}_3)]$. Analogous expressions exist for ρ_2 and ρ_3. If we choose the rotation axis $\hat{\mathbf{u}}$ to be one of the symmetry axes, say, $\hat{\mathbf{z}}$, we have $\rho_3 = 0$. For arbitrary orientation of the boundary $\hat{\mathbf{n}} = (n_1, n_2, n_3)$ the sense vectors of the dislocation lines are specified by

$$\begin{aligned} \hat{\mathbf{r}}_1 &= \frac{1}{(n_1^2+n_3^2)^{1/2}}(-n_3, 0, n_1) \ , \\ \hat{\mathbf{r}}_2 &= \frac{1}{(n_2^2+n_3^2)^{1/2}}(0, -n_3, n_2) \ , \end{aligned} \tag{3.7}$$

when $\rho_i \neq 0$. The dislocations are of mixed character (both edge and screw components) and form a lozenge-shaped mesh in general. Note that for $\hat{\mathbf{n}} = (n_1, n_2, 0)$ (the equatorial plane) the two sets of dislocations are parallel and form an asymmetric tilt boundary. For $\hat{\mathbf{n}} = (0,1,0)$ or $(1,0,0)$ one has only one set of parallel edge dislocations and a symmetric tilt boundary. For $\hat{\mathbf{n}} = (0,0,1)$ one has a twist boundary made up of a square net of screw dislocations.

B. Calculation of $E(\hat{\mathbf{n}})$

In this subsection we outline the calculation of the energy $E(\hat{\mathbf{n}})$ of a grain boundary made up of arrays of dislocation lines specified by the densities and sense vectors derived in Sec. III A. We apply the method used by[5] RS in their calculation of $E(\hat{\mathbf{n}})$ for $\hat{\mathbf{n}} = (n_1, n_2, 0)$ to the general case. $E(\hat{\mathbf{n}})$ consists of the energy required to create the dislocations and the work done in bringing them together due to their mutual interactions. To compute the work done we need the shearing stress on the slip plane (in the slip direction). For a single dislocation this has the expansion[6]

$$\tau = \tau_1\frac{b}{R} + \tau_2\left[\frac{b}{R}\right]^2 + \cdots \ , \tag{3.8}$$

where b is the magnitude of the Burgers vector and R is the distance from the dislocation. Here τ_1 is uniquely determined by the elastic constants and the geometry of the dislocation while the higher-order coefficients depend on the structure of the core and the core—outer-region interactions.

We now evaluate the stresses S_1 and S_2 due to the two sets of dislocations with Burgers vectors $\mathbf{b}_1 = (1,0,0)$ and $\mathbf{b}_2 = (0,1,0)$ respectively. Neither S_1 nor S_2 yield stress fields which vanish at infinity; however, their sum leads to a stress field localized near the boundary. In fact, dislocation networks arising from Frank's formula always give rise to stress-free grains far from the boundary. The energy is obtained by considering one member of the dislocation set 1 and bringing it from infinity and calculating the work done on its slip planes by the stress fields S_1 (self-energy) and S_2 (interaction energy). A similar calculation can be done for the second set. When the two energies are added together the divergent terms cancel and a finite energy per unit area is obtained. The tedious details are provided in the Appendix. The expression for $E(\hat{\mathbf{n}})$ which we calculate is given by

$$\begin{aligned} E(\hat{\mathbf{n}}) &= (\tau_0 b^2/2)\delta E_0[A - \ln\delta] \ , \\ E_0 &= a_1 + a_2 - \nu n_3^2(1/a_1 + 1/a_2) \ , \\ E_0 A &= E_0(A_0 - 1) + n_1^2 a_1 + n_2^2 a_2 - a_1 \ln a_1 - a_2 \ln a_2 \\ &\quad + \nu n_3^2[(\ln a_1)/a_1 + (\ln a_2)/a_2] \ . \end{aligned} \tag{3.9}$$

Here $\tau_0 = G[2\pi(1-\nu)]^{-1}$, G is the shear modulus, ν is Poisson's ratio, $a_1 = (n_1^2+n_3^2)^{1/2}$, and $a_2 = (n_2^2+n_3^2)^{1/2}$. The energy of the atomic misfit in the core region enters through the unknown parameter A_0 which is given by

$$A_0 = 1 + \ln\left[\frac{b}{2\pi r_0}\right] , \tag{3.10}$$

where r_0 is the effective core radius which provides an "ultraviolet cutoff" for the singular behavior of the elastic fields near the dislocation centers.

In carrying out this calculation we make the same assumptions as RS.[5] In particular, as emphasized in the Introduction, the lattice discreteness is ignored in specifying the location of the dislocations. Also, as elucidated in Sec. V, we neglect higher-order terms in δ and take the core radius r_0 to be independent of $\hat{\mathbf{n}}$ and, therefore, independent of the nature of the dislocations.

IV. RESULTS

In this section we discuss the results for the shape of the grain inclusion obtained by applying the Wulff construction (Sec. II) on the grain-boundary energy $E(\theta,\phi)$ derived in Sec. III. We have studied the grain shape $R(\Theta,\Phi)$ at different representative values of Poisson's ratio ν and core-energy constant C (defined later). The shape shows different qualitative features for different ν. There exist at least three ranges of ν: $(0,\nu_c^-)$, (ν_c^-,ν_c^+), and $(\nu_c^+,0.5)$. The critical values ν_c^- and ν_c^+ are functions of C and the range (ν_c^-,ν_c^+) is quite small.

Before proceeding to a discussion of these cases we record some useful properties of $E(\hat{\mathbf{n}})$. There are four equivalent cusps in the Wulff plot[15] at $\theta = \pi/2$, $\phi = 0$, $\pi/2$, π, and $3\pi/2$. These cusps have logarithmically infinite derivatives. They arise, as explained in detail by Read,[6] essentially because the energy per unit length of a dislocation diverges logarithmically with the size of the system. When there is a finite density of dislocations, the distance between dislocations $D \sim 1/(\phi\delta)$ provides an "infrared cutoff" and gives rise to $\ln D \sim \ln[1/(\phi\delta)]$ terms. The cusps give rise to facets in the inclusion shape. In units where $(\tau_0 b^2/2)\delta$ is unity,

$$E(\theta=\pi/2, \phi=0) = A_0 - \ln\delta \equiv C \ . \tag{4.1}$$

For $\theta = \pi/2$ and $\phi = \pi/2$, π, and $3\pi/2$, E has the same value C. Hence, within an overall constant factor, the facets are at a distance C from the center of the grain. Also

$$E(\theta=0,\phi=0)=2(1-\nu)(C-1)\ . \tag{4.2}$$

Clearly this restricts C to be greater than unity. The point $\theta=0,\phi=0$ is an extremum (as is $\theta=\pi,\varphi=0$) and is a minimum for

$$\nu+(3-5\nu)(C-1)<3\ . \tag{4.3}$$

A. $\nu<\nu_c^-$

This regime can be characterized by the fact that the shape in the equatorial plane ($\Theta=\pi/2$) is determined entirely by the Wulff plot in the equatorial plane ($\theta=\pi/2$). We have checked this by performing the Wulff construction in the full three-dimensional space. Let us then for simplicity examine the shape at $\theta=\pi/2$. The energy in the equatorial plane is given by[5]

$$E_e(\phi)=(\tau_0 b^2/2)E_0(A-\ln\delta)\delta\ , \tag{4.4}$$

$$E_0=c+s\ , \tag{4.5}$$

$$A=A_0-cs-\frac{s\ln s+c\ln c}{s+c}\ , \tag{4.6}$$

where $s=|\sin\phi|$ and $c=|\cos\phi|$. Observe that the elastic constants appear in an overall multiplicative constant τ_0. The Wulff plot and the shape for $C=4.0$ are displayed in Figs. 2(a) and 2(b). The shape consists of four flat parts connected by curved regions. The four cusps in the Wulff plot [solid circles on the four axes in Fig. 2(a)] give rise to the flat regions. Setting $\theta=\pi/2$ in Eqs. (2.5) allows one to calculate the curved parts.[14] The portions of the Wulff plot which give rise to the curved segments are shown as solid lines in Fig. 2(a).[15] As discussed in the Introduction the curved parts arise due to the continuum approximation which washes out the extra cusps present in a lattice model with long-ranged interactions. We remark, parenthetically, that if one neglects the ϕ dependence of A (RS point out[5] that this variation is small) the curved parts disappear and one obtains a square in the equatorial plane.

Note that because of the lattice symmetry we can restrict our attention to the range $\phi\in[0,\pi/4]$. It can be shown by using Herring's "tangent circle construction"[13] that, in the case of small ν, the point $\phi=\pi/4$ ($\theta=\pi/2$) on the Wulff plot contributes to the shape of the inclusion. Thus both $\phi=0$ and $\pi/4$ contribute to the shape. It is easy to show that there exists a critical ϕ, ϕ_c, such that $\phi\in(0,\phi_c)$ does not contribute to the shape, while $\phi\in[\phi_c,45°]$ contributes, giving rise to the curved part. In particular ϕ_c determines the corner between the facet and the curved part. Its value is independent of C, G, and τ_0 within our model and is determined by the equation

$$\ln\cos\phi+\sin^2\phi-\cos2\phi(\sin\phi+\cos\phi)\sin\phi=0\ . \tag{4.7}$$

Solving this yields $\phi_c\simeq40.368°$. The corresponding point in the shape Φ_c depends on C and for $C=4$, $\Phi_c\simeq42.616°$. An interesting feature of the shape is the slope discontinuity between the curved and faceted segments. If we measure the discontinuity Δs by the tangent of the angle between the two parts, then $\Delta s=\tan\phi_c\simeq0.850$. In the case of a Wulff plot (for some interfacial free energy f) which has a cusp at ϕ_0, with a finite but discontinuous derivative, the facet length L is proportional to the difference in the slopes

$$\left.\frac{\partial f}{\partial\phi}\right|_{\phi_0^+}-\left.\frac{\partial f}{\partial\phi}\right|_{\phi_0^-}\ .$$

In the grain shape problem, $\partial E/\partial\phi$ is infinite at the cusp. In units where the facet is a distance C from the origin, the length L is given by

$$L=2\left[E_e(\phi_c)\sin\phi_c+\left.\frac{\partial E_e}{\partial\phi}\right|_{\phi_c}\cos\phi_c\right] \tag{4.8a}$$

$$=2(C-0.3197\ldots)\ . \tag{4.8b}$$

Thus the size of the facet increases linearly with C.

We now proceed to discuss the three-dimensional shape, choosing $\nu=0.3$ and $C=4.0$. We use Eq. (2.2) to determine the curved part of the inclusion shape. For a fixed value of $\Phi=\Phi_0$, the boundary of the rounded part is traced [Z versus $\rho=(X^2+Y^2)^{1/2}$] by solving the nonlinear equations

$$Y-X\tan\Phi_0=0\ ,$$

$$Z-Z_0=0\ ,$$

where X, Y, and Z are functions of θ and ϕ. This is done by using a standard routine to find the zeros of nonlinear functions of two variables, exercising care to discard spurious solutions.

In Fig. 3 a sequence of slices of the grain at $\Phi=0°$, 30°, 40°, and 45° are shown. For $\Phi<\Phi_c\simeq42.616°$, the slices intersect the (100) and the ($\bar{1}00$) facets. The top of the grain is smoothly curved as seen from all the figures. The curved and planar regions meet with a slope discontinuity. As Φ increases, the faceted segment decreases, disappearing eventually at $\Phi=\Phi_c$. This is the same value at which the corner between the facet and rounded parts occurs in the equatorial plane. This fact defines this regime in ν. At $\Phi=45°$ the grain is completely rounded. To an excellent approximation the shapes at $\Phi<\Phi_c$ can be obtained from the $\Phi=45°$ shape, which is approximately elliptical, by truncating it with two straight segments parallel to the

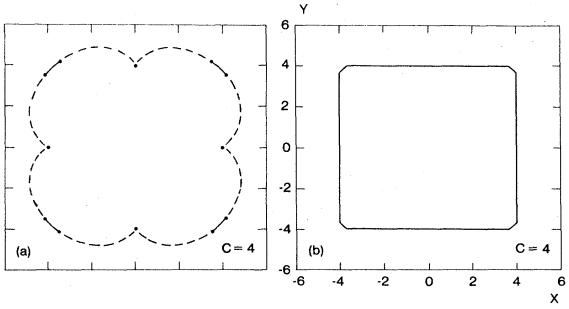

FIG. 2. (a) The Wulff plot $E_e(\phi)$ and (b) the grain shape $R_e(\Phi)$ in the equatorial plane for $C=4.0$. The solid lines in (a) give rise to the curved portions in (b) near $\Phi=\pi/4+n\pi/2$, $n=0,1,2,3$. The points of the cusps in (a) give rise to the four facets in (b). The dashed lines in (a) do not contribute to (b).

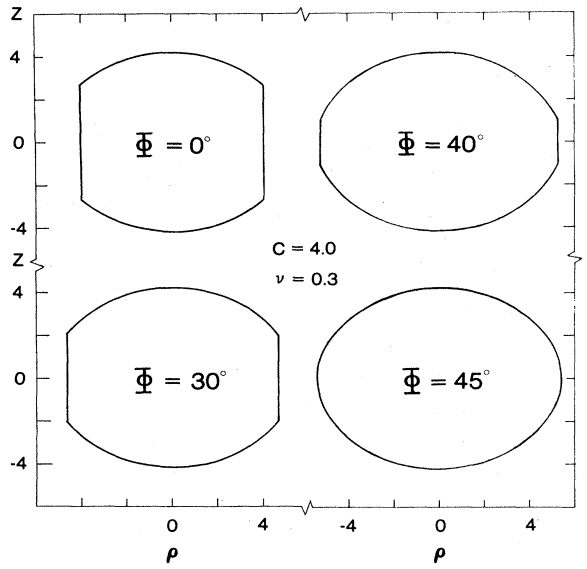

FIG. 3. Slices of the grain shape for fixed azimuthal angle Φ for $C=4.0$ and $\nu=0.3<\nu_c^-$. Note that for $\Phi=45°$, this cut does not intersect any of the four facets, while for the smaller Φ's pictured, portions of the (100) and ($\bar{1}00$) facets appear [cf. Fig. 1(a)].

z axis. The validity of this approximation can be understood by the weak dependence of $E(\hat{\mathbf{n}})$ on ϕ around $\theta=0$. Similar features occur for smaller C, say $C=2.0$, except of course that Φ_c is smaller [$\Phi_c(C=2.0)\simeq 40.035°$].

Now consider the shape viewed in planes at constant Z. For Z small, they are very similar to the shape in the equatorial plane [Fig. 2(b)]. Above $Z=Z_c\simeq 2.644$ ($C=4.0$ and $\nu=0.3$) but below

$$Z=Z_{\max}=4.2[Z_{\max}=2(C-1)(1-\nu)]\ ,$$

the shape is completely rounded. In Fig. 4 we display shapes at two values of Z ($Z=1.5,2.5$), showing how the grain becomes increasingly rounded as Z increases.

To visualize the shape of the grain it is useful to know the outline of the shape of the facet. This can be traced

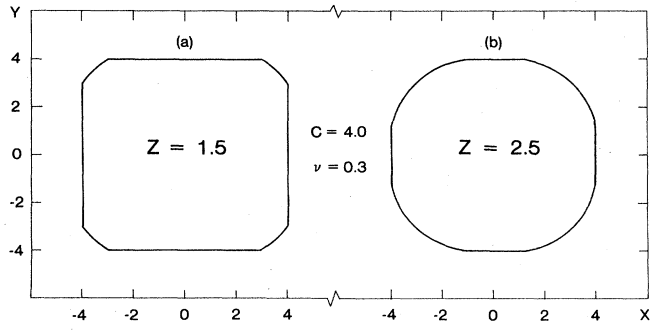

FIG. 4. Slices of the grain shape for fixed Cartesian coordinate Z for $C=4.0$ and $\nu=0.3$. In the equatorial plane, $Z=0$ [Fig. 2(b)]. Since $Z<Z_c$ in both cases, the slices pictured intersect all four facets.

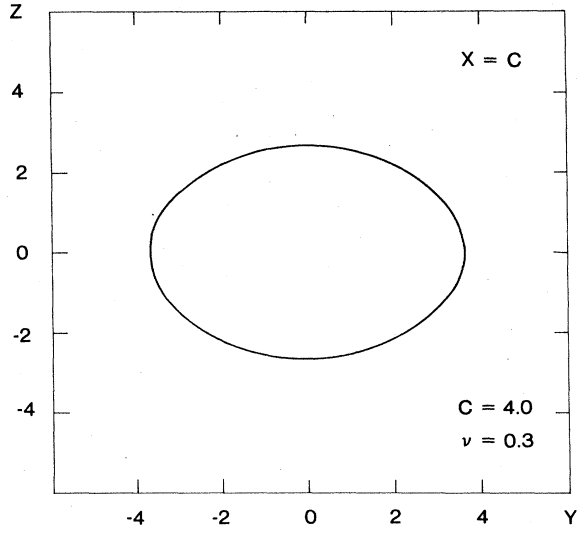

FIG. 5. Shape of any of the four facets for $C=4.0$ and $\nu=0.3<\nu_c^-$. This shape is well approximated by an ellipse.

by solving Eq. (2.2), with X fixed to be equal to C. The shape of the facet is shown in Fig. 5 and is approximately elliptical. Around $Z=0$, the facet shape is quadratic. Thus the complete shape is, to a good approximation, a smoothly curved ellipsoid of revolution truncated by elliptical facets on four sides.

B. $\nu>\nu_c^+$

This regime is characterized by two features of the shape: (i) parts of the shape for $\Theta=\pi/2$ are determined by portions of the Wulff plot with $\theta\neq\pi/2$ and (ii) the curved parts above and below $\Theta=\pi/2$ meet with a slope discontinuity when $\Phi=\pi/4$. Since the $\Phi=45°$ shape is determined by the Wulff plot restricted to $\phi=45°$, we perform Herring's tangent circle construction[13] and analytically determine the critical ν, ν_c^+, above which there is a slope discontinuity at $\Theta=90°$:

$$\nu_c^+=\frac{1}{2}\left[\frac{2C-3+\ln 2}{2C-2+\ln 2}\right]\ .$$

This calculation is performed locally and, hence, $\nu>\nu_c^+$ provides a sufficient condition for the existence of a slope discontinuity. For $C=4$, $\nu_c^+\simeq 0.4253$ while for $C=2$, $\nu_c^+\simeq 0.3143$. We illustrate some of the features of the shape for $C=4$, $\nu=0.45$ ($>\nu_c^+$). In Fig. 6 we show the shape at different values of Φ: 15°, 40°, 42.58°, and 45°. As in the $\nu=0.30$ case (see Fig. 3), the faceted segment decreases in size as Φ increases. If the shape for $\Theta=90°$ (equatorial plane) were entirely determined by the Wulff plot at $\theta=\pi/2$, then the faceted segment would be expected to disappear for Φ greater than $\Phi_{c,\mathrm{eq}}\simeq 42.616°$. However, the three-dimensional calculation yields a critical value of Φ which is smaller, albeit by a tiny amount. Thus at $\Phi=42.58°$ (see Fig. 6), where one might expect a faceted segment, there is none. Also note that for $\Phi>\Phi_c$ (see Fig. 6 for $\Phi=45°$), the smoothly curved parts meet at the equatorial plane with a slope discontinuity as men-

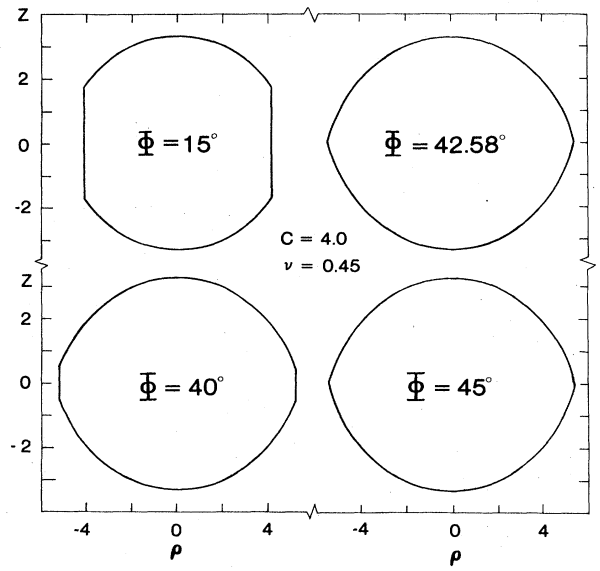

FIG. 6. Slices of the grain shape for fixed azimuthal angle Φ for $C=4.0$ and $\nu=0.45>\nu_c^+$. Note that the cuts which do not intersect any facets exhibit a slope discontinuity in the equatorial plane, unlike the $\nu<\nu_c^-$ case (Fig. 3).

tioned earlier. While such a generic possibility has been pointed out by Herring for the general Wulff construction,[13,16] it is interesting to see it emerge, for the first time, we believe, in an explicit calculation. In Fig. 7 the shape of the facet is shown. In contrast to $\nu<\nu_c^-$ (Fig. 5) the shape is not everywhere smooth—there is a slope discontinuity at $\Theta=\pi/2$.

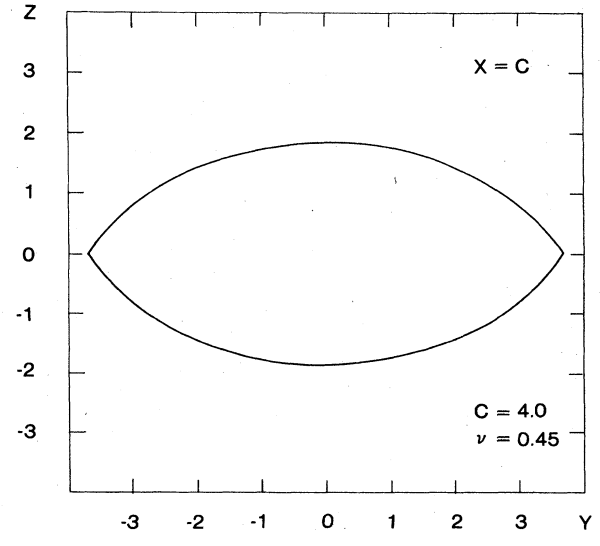

FIG. 7. Shape of any of the four facets for $C=4.0$ and $\nu=0.45>\nu_c^+$. Note that, unlike the $\nu<\nu_c^-$ case (Fig. 5), a slope discontinuity occurs at the equatorial plane in the facet shape [see also Fig. 1(b)].

C. $\nu_c^-<\nu<\nu_c^+$

This regime occupies an extremely small region of ν of the order of 0.02. We point out a result for $\nu\in(\nu_c^-,\nu_c^+)$ merely to show that several qualitatively different features can emerge from the Wulff construction for model systems. The shape is similar to that for $\nu>\nu_c^+$ except that the slice at $\Phi=45°$ shows the section to be completely smooth. Consider the shape as one goes around the equatorial plane *(increasing* Φ from 0 to $\pi/4$). For $\Phi<\Phi_c$ there is a facet. At Φ_c the facet ends. For $\Phi\in(\Phi_c,\Phi_0)$ the curved parts above and below $\Theta=\pi/2$ join at the equatorial plane with a slope discontinuity. For $\pi/4>\Phi>\Phi_0$ the curved parts join at $\Theta=\pi/2$ continuously.

Since the grain-shape nonanalyticities correspond directly to phase transitions,[1,2] we find it helpful to characterize these diverse features in phase-transition language. The boundary of the facet corresponds to a first-order phase transition, as for $\nu<\nu_c^-$ and $\nu>\nu_c^+$. On the equator at $\Phi=\Phi_c$ is a triple point, as for $\nu>\nu_c^+$. The equatorial edge for $\Phi_c<\Phi<\Phi_0$ maps to a first-order boundary. At the end of this first-order boundary $\Phi=\Phi_0$ is a critical point. Surely, in this narrow regime in ν the phase diagram is especially rich. Presumably, as $\nu\to\nu_c^-$ from above, the first-order boundary with its critical point shrinks toward the triple point to form a critical end point at $\nu=\nu_c^-$. Analogously, as $\nu\to\nu_c^+$ from below, the $\Phi_0<45°$ critical point presumably approaches its $\Phi_0>45°$ counterpart until, at $\nu=\nu_c^+$, the points merge so that, for $\nu>\nu_c^+$, only a single first-order boundary remains near $\Phi=45°$.

V. DISCUSSION

The model investigated in Secs. III and IV contains several simplifications which make its solution relatively easy to determine. In this section we investigate in more detail the assumptions of our calculation and explore qualitatively certain effects, neglected in our calculation, which may prove important in a comparison with experiments.

We assume that the angle of rotation δ of the inclusion with respect to the background is small. Others have stated that the expansion in Eq. (3.8) for τ leads to the energy of the grain boundary of the form[6,8,17]

$$E=(\tau_0 b^2/2)E_0\delta(A-\ln\delta+B\delta^2+\cdots)\,. \tag{5.1}$$

For small-angle grain boundaries only the first two terms within the second set of parentheses are retained, as in Eq. (3.9). The coefficient B of the δ^2 term cannot be calculated within elasticity theory. B includes contributions from the interaction between the core and the outer region. Detailed, reliable atomistic estimates for such energies are not available.

In our calculation the inclusion is rotated about the [100] axis of a simple-cubic crystal. The extension to rotations around other axes ($\hat{\mathbf{u}}=[110]$ or [111]) in the simple-cubic case is straightforward if tedious. The case of more realistic crystal structures such as fcc is more complicated: One must take into account the possible dissociation of dislocations into partials and the interaction

between crossing dislocations which can give rise to new configurations. The latter can yield hexagonal nets and these have been observed experimentally.[7] Further, anisotropic elastic constants can give rise to new phenomena since they introduce additional orientation dependence of the grain-boundary energy.

In our model we take the core energy to be independent of the nature of the dislocations. The reliability of this approximation is still, unfortunately, not clear due to the lack of systematic and reliable microscopic calculations of the core energy. One way of taking this into account is the Peierls model where the core cutoff parameter r_0 can be shown to be[7]

$$r_0=\frac{d}{e}\left[\frac{\sin^2\beta}{e^{\gamma(1-\nu)}}+\cos^2\beta\right],$$

where β is the angle between the Burgers vector and the sense vector of the dislocation line, d is some characteristic length scale, and $\gamma=(1-2\nu)/[4(1-\nu)]$. One can use a phenomenological variant in which the relative coefficient of the two terms is an adjustable parameter:

$$r_0=(d/e)[Q\sin^2\beta+\cos^2\beta]\ .$$

Usually the core energies for screw dislocations tend to be larger than those for edge dislocations. We have included this dependence on β in the expression for $E(\hat{\mathbf{n}})$ and performed a few representative calculations of the shape for different values of the parameter Q. For $Q<1$, the screw configuration is favored and this leads to sharper features (first-order transitions between curved parts), while for $Q>1$ the shape is more rounded. This particular connection between Q values and sharp features is presumably only true for rotations around the [001] direction. In general, this core-energy variation will add to the orientation dependence of $E(\hat{\mathbf{n}})$ in a complicated manner. However, it appears that taking a standard model for the core energy (constant r_0), as we have done in the bulk of the calculations of this paper, is reasonable at present.

Our calculation neglects the effect of thermal fluctuations, i.e., entropic contributions to the free energy. Several contributions to the entropy have been considered by others. The configurational entropy due to the position of the core and due to oscillations arising from the possible flexibility of the dislocation line are usually negligible.[18] The vibrational entropy terms appear likely to be most important. The presence of dislocations will alter the frequency of the normal modes of the crystal, predominantly near the cores where Hooke's law fails. Read and Shockley[19] have made a crude estimate of the free-energy change within an Einstein model which contributes additively to C (core-energy term), thereby reducing it. At elevated temperatures, where grain boundaries come to equilibrium, and for low-angle boundaries, the effect is still modest. Since E_0 in Eq. (3.9) arises chiefly from elastically deformed regions, using isothermal elastic constants should be sufficient to take thermal effects into account. Crudely, the decrease in both the elastic constants and the parameter C with temperature lead to more rounded grain shapes. For example, Φ_c where the facet ends in the equatorial plane is 40.035° for $C=2.0$ and decreases to 38.197° for $C=1.50$. The decrease in ν also smooths out sharp corners between curved parts. The question of whether ideal grain boundaries "melt" (roughen) as a function of temperature is open.

We have computed the interfacial energy E by assuming an ideal infinite planar array of dislocations. Effects due to finite size, curvature, and possible nonplanar configurations have been neglected.

We neglect the influence of impurities in our calculation. The effect of impurities on the energy can be discussed qualitatively, as in the case of thermal effects. It is well known that impurities tend to segregate toward boundaries. One experimentally important effect of impurities is their tendency to hinder equilibrium: the motion of the boundary is limited by the diffusion constant for the impurities.

We also assume that the background material is the same as that of the grain. Experimentally, grain shapes are more easily observed in alloy structures (alkali-metal colloids in alkali-halide crystals,[20] rutile in star sapphire,[21] ZrO_2 in magnesia,[22] Al-Al_3Ni eutectics,[23] etc.). These can involve considering the case where the inclusion and the background have different symmetry groups.[24] The simpler case of different lattice constants and different elastic constants but the same symmetry group (which can occur in so-called Widmanstätten structures) has been investigated by methods similar to the one employed in this paper.[25] It appears that in such cases the Wulff construction must be modified, since a strain energy proportional to the volume of the grain contributes in addition to the interfacial free energy.

Our calculation may have indirect applications to the problem of grain shapes in polycrystalline samples. This problem has been understood in the limit in which the orientation dependence of the grain-boundary energy is neglected,[26] in which it becomes equivalent to the shape of a froth of soap bubbles.[27] Mathematically the problem is formulated as a constrained minimization of the total intergranular free energy with fixed (in general, different) volumes for each of the grains. Although a proof is lacking, in two dimensions it appears that a portion of the global shape between two adjacent grains will correspond to a particular piece of the grain shape of an inclusion of one of these grains in the background of the other. Complications arise in three dimensions due to the tiling of space with inclusion shapes. Nevertheless, it seems possible that portions of the shapes we calculate may be closely related to the boundary between two nearly aligned grains in a polycrystalline sample. An investigation of the relevance of this mathematical formulation to experimental situations, incorporating the relevant experimental time scales, seems important at present.

Note added. The shape in the equatorial plane ($\theta=\pi/2$) has been calculated by Smith and Hazzledine.[28]

ACKNOWLEDGMENTS

We owe special thanks to M. Wortis for numerous insightful conversations. We also acknowledge useful conversations with Professor J. Hirth, Professor W. F. Saam, and A.-C. Shih. One of us (C.J.) would like to thank the

A. P. Sloan Foundation for support. He is grateful to Dr. P. M. Horn for his hospitality at the IBM T. J. Watson Research Center. Another of us (C.R.) wishes to acknowledge The Ohio State University for support.

APPENDIX: DETAILS OF THE CALCULATION OF Eq. (3.9)

We define a reference lattice frame $OXYZ$ as a coordinate frame whose axes are along the three crystal axes of a simple-cubic crystal. In this frame, consider a grain-boundary plane with normal $\hat{\mathbf{n}}=(n_1,n_2,n_3)$ obtained by rotating two crystals by $\theta/2$ and $-\theta/2$ about the $\hat{\mathbf{z}}$ axis, respectively. In general, we will have two sets of dislocation lines in the plane along the directions

$$\hat{\mathbf{r}}_1=\frac{1}{(n_1^2+n_3^2)^{1/2}}(-n_3,0,n_1)$$

and

$$\hat{\mathbf{r}}_2=\frac{1}{(n_2^2+n_3^2)^{1/2}}(0,-n_3,n_2)$$

with Burgers vectors $\mathbf{b}_1=(1,0,0)$ and $\mathbf{b}_2=(0,1,0)$, respectively. The separation between dislocations in the two sets is

$$D_1=\frac{1}{\theta(n_1^2+n_3^2)^{1/2}}\ ,\quad D_2=\frac{1}{\theta(n_2^2+n_3^2)^{1/2}}\ .$$

The grain-boundary energy can be obtained by calculating the energy due to these two sets of dislocation; this can be done by integrating the shear stress over the slip planes.

It is convenient to introduce two other coordinate frames: $Oxyz$ with $\hat{\mathbf{z}}$ along $\hat{\mathbf{r}}_1$ direction and $Ox'y'z'$ with $\hat{\mathbf{z}}'$ along that of $\hat{\mathbf{r}}_2$. $\hat{\mathbf{x}}$ and $\mathbf{x}'$ are fixed by choosing $\mathbf{b}_1\cdot\hat{\mathbf{y}}=0$ and $\mathbf{b}_2\cdot\hat{\mathbf{x}}'=0$. If we define

$$\sin\alpha\equiv\frac{-n_3}{(n_1^2+n_3^2)^{1/2}},\quad \cos\alpha\equiv\frac{n_1}{(n_1^2+n_3^2)^{1/2}}\ ,$$
$$\sin\beta\equiv\frac{-n_3}{(n_2^2+n_3^2)^{1/2}},\quad \cos\beta\equiv\frac{n_2}{(n_2^2+n_3^2)^{1/2}}\ , \tag{A1}$$

then the orthogonal transformations that rotate $OXYZ$ to $Oxyz$ and $Ox'y'z'$ are given by

$$T_1=\begin{bmatrix}\cos\alpha & 0 & -\sin\alpha\\ 0 & 1 & 0\\ \sin\alpha & 0 & \cos\alpha\end{bmatrix},$$
$$T_2=\begin{bmatrix}1 & 0 & 0\\ 0 & \cos\beta & -\sin\beta\\ 0 & \sin\beta & \cos\beta\end{bmatrix}, \tag{A2}$$

respectively. The transformation matrix between the two frames is

$$R=T_2T_1^{-1}\ . \tag{A3}$$

In the $Oxyz$ frame, since the set-1 dislocations are along $\hat{\mathbf{z}}$ we know how to sum their stress fields by introducing a complex representation (RS).[5] Let $r=x+iy$ and $z_1=D_1e^{i\phi}$, where ϕ is the angle between the boundary and the $\hat{\mathbf{x}}$ axis (now the boundary is parallel to $\hat{\mathbf{z}}$). We have, at point (x,y), the stress field due to these infinite dislocations

$$\tau_{xy}^{(1)}=\sum_{n=-\infty}^{\infty}\frac{x_n(x_n^2-y_n^2)}{(x_n^2+y_n^2)^2}b_{1e}=\mathrm{Re}\left[\frac{\pi}{z_1^2}\left[D_1\cos\phi\,\mathrm{ctg}\frac{\pi r}{z_1}-iD_1(y\cos\phi-x\sin\phi)\frac{\pi}{z_1}\csc^2\frac{\pi r}{z_1}\right]\right]b_{1e}\ , \tag{A4}$$

$$\tau_{yz}^{(1)}=\sum_{n=-\infty}^{\infty}\frac{x_n}{(x_n^2+y_n^2)}(1-\nu)b_{1s}=\mathrm{Re}\left[(1-\nu)\frac{\pi}{z_1}\,\mathrm{ctg}\frac{\pi r}{z_1}\right]b_{1s}\ , \tag{A5}$$

where $x_n=x+nD_1\cos\phi$, $y_n=y+nD_1\sin\phi$. Also $b_{1s}=\sin\alpha$ and $b_{1e}=\cos\alpha$ are screw and edge components of the Burgers vector of the first set dislocations. We have set $G/2\pi(1-\nu)=1$ and $b=1$.

The self-energy (per unit area) of set-1 dislocations is obtained by integrating

$$E_s^{(1)}=\frac{1}{2D_1}\int_{r_0}^{R}(\tau_{xy}^{(1)}b_{1e}+\tau_{yz}^{(1)}b_{1s})dx$$
$$=\frac{1}{2D_1}\cos^2\alpha\left[\frac{\pi R}{D_1}\cos\phi\sin2\phi-\ln\left[\frac{2\pi r_0}{D_1}\right]+\sin^2\phi\right]+\frac{1-\nu}{2D_1}\sin^2\alpha\left[\frac{\pi R}{D_1}\sin\phi-\ln\left[\frac{2\pi r_0}{D_1}\right]\right], \tag{A6}$$

where r_0 is the core radius.

The interaction energy between the two sets of dislocation is found by calculating the work done in bringing in one member of set 2 in the presence of all set-1 dislocations. The interaction energy per unit area is obtained by dividing by the product of the length of the dislocation lines and the distance between the second set dislocations. Since the stress field due to set-1 dislocations is periodic in the z' direction with period $\Delta=D_1/\sin\psi$, where $\cos\psi=\hat{\mathbf{z}}\cdot\hat{\mathbf{z}}'$, we obtain, in the $Ox'y'z'$ frame,

$$E_{\mathrm{int}}^{(1)}=\frac{1}{2D_2}\frac{1}{\Delta}\int_d^{d+\Delta}dz'\int_{y_0'}^{y_0'+R}dy'(\tau_{x'y'}^{(1)}b_{2e}+\tau_{x'z'}^{(1)}b_{2s})\ ,$$

where d is some constant. $\tau_{x'y'}^{(1)}b_{2e}+\tau_{x'z'}^{(1)}b_{2s}$ can be expressed in terms of stress field in $Oxyz$ frame. Since we know the transformation matrix R,

$$E_{\mathrm{int}}^{(1)}=\frac{1}{2D_2}\frac{1}{\Delta}\int_d^{d+\Delta}dz'\int_{y_0'}^{y_0'+R}(\cos\alpha\tau_{xy}^{(1)}+\sin\alpha\tau_{yz}^{(1)})dy'\ .$$

By transforming (x,y,z) to (x',y',z') and carrying out the integration, we obtain

$$E_{\rm int}^{(1)} = -\frac{\pi R}{2D_1D_2}\cos^2\alpha\cos\phi\sin 2\phi - \frac{\pi R}{2D_1D_2}(1-\nu)\sin^2\alpha\sin\phi\ .$$

We can carry out the same calculation for set-2 dislocations. The result is the same except for changing $D_1\to D_2$, $D_2\to D_1$, $\phi\to\pi/2-\phi'$, and $\alpha\to\beta$, where ϕ' is the angle between grain boundary and $\hat{\mathbf{x}}'$ axis. We have

$$E_s^{(2)} = \frac{1}{2D_2}\cos^2\beta\left[\frac{\pi R}{D_2}\sin\phi'\sin 2\phi' - \ln\left[\frac{2\pi r_0}{D_2}\right] + \cos^2\phi'\right] + \frac{(1-\nu)}{2D_2}\sin^2\beta\left[\frac{\pi R}{D_2}\cos\phi' - \ln\left[\frac{2\pi r_0}{D_2}\right]\right],$$

$$E_{\rm int}^{(2)} = -\frac{\pi R}{2D_1D_2}\cos^2\beta\sin\phi'\sin 2\phi' - \frac{\pi R}{2D_1D_2}(1-\nu)\sin^2\beta\cos\phi'\ .$$

So, we obtain the final expression for energy

$$E = E_s^{(1)} + E_s^{(2)} + E_{\rm int}^{(1)} + E_{\rm int}^{(2)} = E_0\theta(A - \ln\theta)\ ,$$

where[29]

$$E_0 = \tfrac{1}{2}[(n_1^2+n_3^2)^{1/2} + (n_2^2+n_3^2)^{1/2}] - \frac{\nu}{2}\left[\frac{n_3^2}{(n_1^2+n_3^2)^{1/2}} + \frac{n_3^2}{(n_2^2+n_3^2)^{1/2}}\right],$$

$$E_0A = \tfrac{1}{2}[(n_1^2+n_3^2)^{1/2}n_1^2 + (n_2^2+n_3^2)^{1/2}n_3^2] - E_0\ln\left[\frac{2\pi r_0}{b}\right]$$
$$- \tfrac{1}{2}\{(n_1^2+n_3^2)^{1/2}\ln[(n_1^2+n_3^2)^{1/2}] + (n_2^2+n_3^2)^{1/2}\ln[(n_2^2+n_3^2)^{1/2}]\}$$
$$+ \frac{\nu}{2}\left[\frac{n_3^2}{(n_1^2+n_3^2)^{1/2}}\ln[(n_1^2+n_3^2)^{1/2}] + \frac{n_3^2}{(n_2^2+n_3^2)^{1/2}}\ln[(n_2^2+n_3^2)^{1/2}]\right].$$

Setting $Gb^2/2\pi(1-\nu)$ back in, we obtain Eq. (3.9).

Rey and Saada[30] have calculated the elastic energy for two sets of parallel infinite dislocations. It can be shown that their value of E_0A disagrees with ours for all $\hat{\mathbf{n}}$ except $\hat{\mathbf{n}}=(0,0,1)$. We believe that our expression is correct and in a future publication[31] we plan to discuss this discrepancy.

[1] C. Rottman and M. Wortis, Phys. Rep. **103**, 59 (1984).

[2] A. F. Andreev, Zh. Eksp. Teor. Fiz. **80**, 2042 (1981) [Sov. Phys.—JETP **53**, 1063 (1982)].

[3] C. Jayaprakash, W. F. Saam, and S. Teitel, Phys. Rev. Lett. **50**, 2017 (1983); C. Rottman and M. Wortis, Phys. Rev. B **29**, 328 (1984); C. Jayaprakash and W. F. Saam, *ibid.* **30**, 3916 (1984); C. Jayaprakash, C. Rottman, and W. F. Saam, *ibid.* **30**, 6549 (1984).

[4] C. Rottman, M. Wortis, J. D. Heyraud, and J. J. Métois, Phys. Rev. Lett. **52**, 1009 (1984); S. Balibar, P. E. Wolf, and F. Gallet, Physica (Utrecht) **106A**, 138 (1984); T. Onachi and I. Taniguchi, J. Cryst. Growth **65**, 84 (1983), and unpublished.

[5] W. T. Read and W. Shockley, Phys. Rev. **78**, 275 (1950).

[6] W. T. Read, *Dislocations in Crystals* (McGraw-Hill, New York, 1953).

[7] J. P. Hirth and J. Lothe, *Theory of Dislocations*, 2nd ed. (Wiley-Interscience, New York, 1982).

[8] H. Brooks, in *Metal Interfaces* (American Society for Metals, Cleveland, 1952), p. 20ff.

[9] The application of the Wulff construction to such problems appears first to have been made by C. Herring, in *The Physics of Powder Metallurgy*, edited by W. E. Kingston (McGraw-Hill, New York, 1951), p. 143ff.

[10] Facet-to-curved-surface transitions have also been proposed for ECS models at nonzero temperature. See Refs. 1 and 3.

[11] An excellent pedagogical discussion of the Wulff construction may be found by R. K. P. Zia, in Proceedings of the 26th Scottish Universities Summer School in Physics, 1983, edited by K. Bowler and A. McKane (unpublished).

[12] E. M. Lifshitz and L. P. Pitaevskii, *Statistical Physics, Part I* (Pergamon, Oxford, 1980), pp. 520–524.

[13] C. Herring, Phys. Rev. **82**, 87 (1951).

[14] W. K. Burton, N. Cabrera, and F. C. Frank, Philos. Trans. R. Soc. London, Ser. A **243**, 299 (1951), Appendix D.

[15] Since we work at $T=0$, it is possible to find $E(\hat{n})$ for orientations $\hat{n}$ which do *not* appear in the inclusion shape. When we speak of the Wulff plot, we imagine that it includes portions for these unstable orientations as well as the usual pieces corresponding to orientations which appear in the inclusion shape. For a discussion of these "passive" regions, see Ref. 1.

[16] C. Herring, in *Structure and Properties of Solid Surfaces*, edited by R. Gomer and C. S. Smith (University of Chicago, Chi-

cago, 1953), p. 5ff.

[17]Although both Refs. 6 and 8 claim this result, they give the credit for the proof of this to each other. To the best of our knowledge *no* mechanism gives rise to an additional term to Eq. (5.1) of lower order than the $B\delta^2$ term.

[18]F. C. Frank, Nuovo Cimento Suppl. **7**, 386 (1958); A. H. Cottrell, *Dislocations and Plastic Flow in Crystals* (Oxford University, London, 1953).

[19]W. Shockley, in *L'état Solide: Rapports et Discussions,* edited by R. Stoops (Bruxelles, 1952), p. 431ff; W. T. Read and W. Shockley, in *Imperfections in Nearly Perfect Crystals* (Wiley, New York, 1952), p. 352ff.

[20]G. Chassagne, D. Durand, J. Serughetti, and L. W. Hobbs, Phys. Status Solidi A **40**, 629 (1977).

[21]D. S. Phillips, A. H. Heuer, and T. E. Mitchell, Philos. Mag. A **42**, 385 (1980).

[22]A. H. Heuer and T. E. Mitchell, in *Precipitation Processes in Ceramics,* edited by K. C. Russell and M. I. Aaronson (Metallurgical Society of AIME, 1978).

[23]F. D. Lemkey, R. W. Hertzberg, and J. A. Ford, Trans. Metall. Soc. AIME **233**, 334 (1965).

[24]Symmetry constraints on the interfacial free energy in such cases has been investigated in detail by G. Kalonji and J. W. Cahn, J. Phys. (Paris), Colloq. **43**, C6-25 (1982). See also G. Kalonji, Ph.D. thesis, MIT, 1982.

[25]Y. He and C. Jayaprakash (unpublished); A.-C. Shi and M. Wortis (private communication).

[26]C. S. Smith, Metall. Rev. **9**, 1 (1964); in *Metal Interfaces* (American Society for Metals, Cleveland, 1952), p. 65ff; D. McLean, *Grain Boundaries in Metals* (Oxford University, Oxford, 1957).

[27]F. J. Almgren and J. E. Taylor, Sci. Am. **235**(1), 82 (1976).

[28]D. A. Smith and P. M. Hazzledine, Scr. Metall. **15**, 393 (1981).

[29]The expression for E_0 is given in Chap. 12, problem 6 in Ref. 6.

[30]C. Rey and G. Saada, J. Phys. (Paris) **38**, 721 (1977).

[31]Y. He, C. Jayaprakash, C. Rottman, A.-C. Shi, and M. Wortis (unpublished).